

# Empirical relation between angular momentum transport and thermal-to-magnetic pressure ratio in shearing box simulations

E.G. Blackman<sup>1</sup> R.F. Penna<sup>1</sup>, P. Varnière<sup>1,2</sup>

1. *Dept. of Physics and Astronomy, University of Rochester, Rochester NY 14627, USA;*

2. *LAOG, Université J. Fourier UMR 5571, France*

## ABSTRACT

By combining data from four different sets of published 3-D simulations of Keplerian shearing boxes unstable to the magnetorotational instability (MRI), we highlight tight anti-correlations between the total effective inferred angular momentum transport parameter,  $\alpha_{tot}$ , its separate Maxwell and Reynolds contributions  $\alpha_{mag}$  and  $\alpha_{kin}$ , and the kinetic to magnetic pressure ratio  $\beta$ . Plots of  $\text{Log}(\alpha_{kin})$ ,  $\text{Log}(\alpha_{mag})$ , and  $\text{Log}(\alpha_{tot})$  vs  $\text{Log}(\beta)$  are straight lines even as  $\alpha_{kin}$ ,  $\alpha_{mag}$ , and  $\alpha_{tot}$  vary by four orders of magnitude for the full range of simulations included. The ratio  $\alpha_{kin}/\alpha_{mag}$  and the product  $\alpha_{tot}\beta$  are therefore remarkably constant over this range, the latter maintaining a value between 0.4–0.5 independent of the presence or absence of weak mean fields, the simulation method, and the choice of initial and boundary conditions, with possibly a slight dependence on polytropic index. Although more work is needed to derive  $\alpha_{tot}\beta$  from first principles, the simulations tightly constrain this product even though they do not strongly constrain  $\alpha_{tot}$  and  $\beta$  separately.

(submitted to MNRAS)

**Key Words:** accretion disks–magnetic fields–magnetohydrodynamics (MHD)–instabilities

## 1. Introduction

Accretion disks are widely appreciated to be a source of emission from gas or plasma orbiting central stars or compact objects (c.f. Frank, King, Raine 1992). In order to explain the rapid variability and short lifetimes of accreting systems without unphysical mass densities, some enhanced angular momentum transport beyond that which can be supplied by the microphysical transport coefficients is typically required. For sufficiently ionized disks, the magneto-rotational instability (MRI) offers a solution to this problem for sufficiently ionized disks (e.g. Balbus & Hawley 1991; 1998).

The MRI feeds off of an initially weak magnetic field and the turbulence induced by the ensuing instability amplifies the fluctuating magnetic energy by line stretching. Sustained magnetic fields under the influence of a shear flow in a radially decreasing angular velocity profile produce a negative magnetic (Maxwell) stress, which, in principle, produces the dominant positive outward angular momentum transport. 3-D Simulations (e.g. Hawley, Gammie, Balbus, 1995, 1996; Brandenburg et al. 1995; Stone et al. 1995) have revealed that the nonlinear evolution of systems unstable to the MRI leads to a Maxwell stress whose magnitude is larger than the negatively signed Reynolds stress. The MRI sustains the turbulent Maxwell stress and thus the outward angular momentum transport.

While the MRI has been numerically shown to provide an effective turbulent magnetic stress, incorporating the saturated state of the MRI into the framework of practical accretion disc modeling using, for example the  $\alpha_{tot}$  viscosity coefficient formalism (Shakura & Sunyaev 1973), where  $\alpha_{tot}$  is defined from the turbulent viscosity,  $\nu_T = \alpha_{tot} c_s H$  and  $c_s$  and  $H$  are the sound speed and disk scale height) suffers from the non-universality of values of  $\alpha_{tot}$  inferred from simulations. Depending on the boundary conditions, initial conditions, different treatments of viscosity and resistivity, and the presence or absence of stratification, the values inferred from simulation can vary by 4 orders of magnitude (see Tables 1-5). However, the  $\alpha_{tot}$  prescription provides a practical mean field formalism that allows a straightforward calculation of accretion disk spectra for comparison to observations by parameterizing non-linear correlations of turbulent fluctuations by a simple closure. Developing an improved mean field theory that also incorporates the physics of the MRI, while still being practical is an important target of recent and ongoing work (e.g. Ogilvie 2003; Pessah 2006ab).

Here we emphasize that the ratio of the thermal to magnetic pressure,  $\beta$  is not generally an independent function of  $\alpha_{tot}$ , even though it is sometimes assumed to be in phenomenological analytic disc models (e.g. Yuan et al. 2005). In this paper we combine the published data listed in the simulations of Table 1 to determine the empirical correlation between the kinetic and magnetic contributions to  $\alpha_{tot}$ .

In Sec. 2 we derive the formalism that relates the kinetic and magnetic parts of  $\alpha_{tot}$  to  $\beta$  for different adiabatic indices and give a physical argument for an inverse relation between  $\alpha_{tot}$  and  $\beta$ . We do not present a rigorous theory in the present work as our main focus is empirical. Toward this end, in Sec. 3 we plot the data points from published simulations and infer the empirical values for the quantities defined in Sec. 2. The data reveal that the product  $\alpha_{tot}\beta$  is a constant. We conclude in Sec. 4.

## 2. Maxwell and Reynolds Contributions to Transport and Relations to $\beta$

In the steady-state, ignoring microphysical viscosity, the mean azimuthal momentum equation is given by (e.g. Balbus & Hawley 1998)

$$\nabla \cdot \left[ r\rho v_\phi \mathbf{v} - r \frac{B_\phi}{4\pi} \mathbf{B}_p + r \left( P + \frac{B_p^2}{8\pi} \right) \mathbf{e}_\phi \right] = 0 \quad (1)$$

The quantity inside the brackets represents the flux of angular momentum. Of particular interest is the  $r\phi$  component of this flux, which, when greater than zero, represents the outward radial transport of angular momentum. It is given by

$$F_{r\phi} = \left[ r\rho v_\phi v_r - r \frac{B_\phi}{4\pi} B_r \right]. \quad (2)$$

Because axisymmetric accretion disk equations formally represent mean field equations, we are interested in the averaged value of  $F_{r\phi}$ . Toward obtaining this, we split the magnetic field and velocity into mean (indicated by an overbar) and fluctuating components (indicated by lower case). As in Balbus & Hawley (1998), we take the mean to represent a height integration over all  $z$ , an average over all  $\phi$  and an average over some fixed range of  $r$ . For a quantity  $Q = \overline{Q} + q$  we have  $\langle q \rangle = 0$  and

$$\langle Q \rangle = \overline{Q} = \frac{\int Q \rho d\phi dr dz}{2\pi \Sigma \Delta r}, \quad (3)$$

where  $\Sigma = \int_{-H}^H \rho dz$ . Assuming that  $\rho = \overline{\rho}$  (no fluctuating density), applying (3) to (2) gives

$$\overline{F}_{r\phi} = \frac{\Sigma R}{2H} \left[ \overline{V}_\phi \overline{V}_r - \overline{V}_{A,\phi} \overline{V}_{A,r} + \langle v_\phi v_r \rangle - \langle b_\phi b_r \rangle \right], \quad (4)$$

where  $\overline{\mathbf{V}}_A$  is the Alfvén velocity associated with the mean field and  $\mathbf{b}$  is the Alfvén velocity associated with the fluctuating field. The first term on the right is an inward flux of angular momentum, since  $\overline{V}_r < 0$  and  $\overline{V}_\phi > 0$  at the inner most radii for an accretion disc. The remaining terms must provide the needed outward transport of angular momentum if matter is to accrete. The last two terms represent purely turbulent transport. In what follows, we assume that the mean magnetic field of smaller magnitude than the fluctuating field in saturation and that the dominant angular momentum transport comes from the last two terms of (4). (This is consistent with all of the simulations we consider.)

The shearing box simulations of Table 1 employ local Cartesian coordinates in the rotating frame. In this shearing-sheet approximation, the mean velocity  $\overline{V}_y$  vanishes at the inner most radius  $r_0$  of the shearing box, and points in the  $-\hat{\mathbf{y}}$  for  $x = r - r_0 > 0$ , decreasing

outward in Keplerian fashion such that  $\bar{V}_y = \frac{\partial \tilde{\Omega}}{\partial r} \frac{r-r_0}{r_0} r \simeq -\frac{3}{2} \tilde{\Omega} x$ . Here  $\tilde{\Omega}$  is the local orbital speed,  $\Omega$  is the orbital speed of the rotating frame,  $x \equiv r - r_0$ , and  $x \ll r_0$ . In this context, we can combine the last 2 contributions of (4) into a Cartesian stress tensor

$$\bar{W}_{xy} \equiv \langle v_y v_x \rangle - \langle b_y b_x \rangle. \quad (5)$$

Using the Shakura-Sunayev prescription of  $\nu_T \equiv \alpha_{tot} c_s H$  of Sec. 1, the stress for a Keplerian flow in a shearing box that corresponds to an outward flux of angular momentum is

$$-\nu_{eff} \partial_x \bar{V}_y \simeq \frac{3}{2} \Omega \alpha_{tot} c_s H. \quad (6)$$

Setting this equal to (5) gives a closure for the stress tensor, so that

$$\alpha_{tot} = \frac{2\bar{W}_{xy}}{3\Omega c_s H} = \frac{2f(\Gamma) \bar{W}_{xy}}{3c_s^2}, \quad (7)$$

where  $\Gamma$  is the polytropic index and  $f(1) = \sqrt{\frac{1}{2}}$  (isothermal) and  $f(5/3) = \sqrt{\frac{1}{3}}$  (adiabatic). The last relation in (7) comes from solving the equation of hydrostatic equilibrium, namely

$$\frac{1}{\bar{\rho}} \frac{\partial \bar{P}}{\partial z} \simeq -\frac{GM}{R^2} \frac{z}{R}. \quad (8)$$

Over a density scale height, the solution gives  $\Omega H = \frac{c_s}{f(\Gamma)}$ , with midplane sound speed  $c_s$ .

We now split (7) into magnetic and kinetic terms such that  $\alpha_{tot} = \alpha_{kin} + \alpha_{mag}$  where

$$\alpha_{mag} \equiv -\frac{2f(\Gamma) \langle b_y b_x \rangle}{3c_s^2} = \frac{C_{mag}(\Gamma, \beta)}{\beta}, \quad (9)$$

and

$$\alpha_{kin} \equiv \frac{2f(\Gamma) \langle v_y v_x \rangle}{3c_s^2} \equiv \frac{C_{kin}(\Gamma, \beta)}{\beta}, \quad (10)$$

where  $C_{mag}(\Gamma, \beta) \equiv -\frac{4f(\Gamma)}{3\Gamma} \frac{\langle b_x b_y \rangle}{\langle b^2 \rangle}$  and  $C_{kin}(\Gamma, \beta) \equiv \frac{4f(\Gamma)}{3\Gamma} \frac{\langle v_x v_y \rangle}{\langle v^2 \rangle}$  are to be inferred from the data. We also define  $C_{tot}(\Gamma, \beta)$  such that  $\alpha_{tot} = C_{tot}/\beta$ . The statistically determined  $C_{tot}$  need not exactly equal the separately determined best fit values of  $C_{mag}$  and  $C_{kin}$ .

Before discussing the data, we provide a crude physical argument which anticipates a strong anti-correlation between  $\alpha_{tot}$  and  $\beta$ . Note that  $\nu_{eff} = \alpha_{tot} c_s H = v_T L$ , where  $v_T$  and  $L$  are a turbulent velocity and dominant energy containing fluctuation scale. In a turbulent flow, the ratio of magnetic to kinetic turbulent energies is typically of order unity in saturation (and actually slightly larger than unity for MRI simulations). Crudely, if  $v_A \sim v_T$ , then  $\alpha_{tot} c_s H \sim v_A L$ . But  $L \sim v_T/\Omega \sim v_A/\Omega$ , if the eddy turnover time scale is comparable to the orbit time. The latter is a reasonable assumption since the growth rate for a MRI instability that initiates turbulence is of order the rotation rate. We therefore have  $\alpha_{tot} c_s H \sim v_A^2/\Omega$  which implies  $\alpha_{tot} \sim \frac{2f(\Gamma)}{\Gamma \beta}$ , using the relations below Eq. (8). The specific anisotropy due to Keplerian shear likely implies a missing factor of order unity.

### 3. The $\alpha(\beta)$ Relation from Published Numerical Simulation Data

We have used the 4 sets of shearing box simulations listed in Table 1. The data from each reference used are presented in each of the tables 2, 3, 4, and 5. Brandenburg et al. 1995’s stratified simulations differ from the other 3 in that vertical field boundaries were used at the top and bottom of the box. This allowed mean field amplification to occur, in contrast to the periodic boundary conditions used in the other 3 cases of Table 1. However, since the mean field saturated at values relatively small compared to the random field, the effect of mean field growth on the total stress is relatively small.

In Fig. 1 we plot  $\log \alpha_{kin}$  and  $\log \alpha_{mag}$  vs.  $\log \beta$  separately for the  $\Gamma = 5/3$  simulations (top row) and  $\Gamma = 1$  cases (bottom row). The plots include all of the data in Tables 2, 3, 4, and 5 except for the last row of Table 4, which involves ambipolar diffusion and thereby deviates from the basic MHD case.

The best fit solid lines are shown, with the equations for these lines at the top of each panel in Figs. 1 and 2. For each panel, the fit at the top is of the form  $\log(\alpha) = A \log(\beta) + D$ , shown at the top with  $A$  and  $D$  constants. Note that the correlation coefficients  $R^2$  are generally near unity. We can use these fits to extract best fit values of  $C_{mag}(\Gamma, \beta)$  and  $C_{kin}(\Gamma, \beta)$  defined in Sec. 2. Clockwise from the top left panel of Fig. 1 we then have

$$C_{kin}(5/3, \beta) = 10^{-0.966} \beta^{0.049} \quad (11)$$

$$C_{mag}(5/3, \beta) = 10^{-0.426} \beta^{0.059}, \quad (12)$$

$$C_{mag}(1, \beta) = 10^{-0.402} \beta^{-0.11}, \quad (13)$$

and

$$C_{kin}(1, \beta) = 10^{-1.37} \beta^{0.132}. \quad (14)$$

For Fig. 2 we have for the left and right panels respectively,

$$C_{tot}(5/3, \beta) = 10^{-0.328} \beta^{0.074} \quad (15)$$

and

$$C_{tot}(1, \beta) = 10^{-0.397} \beta^{-0.05}. \quad (16)$$

Given the very weak dependencies on  $\beta$  of these latter two formulae, the results imply that  $C_{5/3, \beta} \sim 0.47$  and  $C_{1, \beta} \sim 0.40$  are essentially independent of  $\beta$ . The fits therefore show that  $\alpha_{tot} \sim \frac{(0.4, 0.5)}{\beta}$  as  $\alpha_{tot}$  varies by over 4 orders of magnitude between simulations that use different methods, and different initial and boundary conditions.

Similar best fits can be performed to infer the best fit of  $\alpha_{kin}/\alpha_{mag}$ . Here we instead give the ratio of separate best fits to  $\alpha_{kin}$  to  $\alpha_{mag}$  using (11-14) in the form  $C_{kin, \Gamma}/C_{mag, \Gamma}$ . For

$\Gamma = 5/3$ , using (11) and (12) we have  $C_{kin,5/3}/C_{mag,5/3} \simeq 0.29\beta^{-0.01}$  exhibiting a negligible dependence on  $\beta$ . For  $\Gamma = 1$ , Eqs. (14) and (13) give  $C_{kin,1}/C_{mag,1} \simeq 0.11\beta^{0.242}$  which shows a stronger dependence on  $\beta$  but there is less data for  $\Gamma = 1$  than for  $\Gamma = 5/3$ . The near constancy of  $\alpha_{kin}/\alpha_{mag}$  was also noted by (Pessah et al. 2006ab).

#### 4. Conclusion

We have highlighted that data from published shearing box MRI simulations (Tables 1-5) show tight anti-correlations of  $\beta$  with  $\alpha_{mag}$ ,  $\alpha_{kin}$ , and their sum  $\alpha_{tot}$ . In particular, the product  $\alpha_{tot}\beta \sim 0.4 - 0.5$ , even as  $\alpha_{tot}$  varies by over 4 orders of magnitude between simulations. The data were taken from simulations invoking different vertical boundary conditions, different initial conditions, the presence or absence of stratification, explicit vs. numerical viscosity, and different polytropic indices.

The fact that no universal value of  $\alpha_{tot}$  emerges from these simulations implies that boundary and initial conditions are influencing its value and restricting phase space. It perhaps remarkable therefore, that the product of  $\alpha_{tot}$  and  $\beta$  is so constant. The specific value of the constant likely depends on those features identical in all simulations, such as the Keplerian shear. This is consistent with what one might expect from the argument in the last paragraph of Sec. 2, analysis of the linear regime (Pessah et al. 2006a), and more general nonlinear closures (e.g. Ogilvie 2003; Pessah et al. 2006b). More work is needed to determine the constant  $\alpha_{tot}\beta$  from first principles. Alternatively, the constants  $\alpha_{tot}\beta$  and  $\alpha_{mag}/\alpha_{kin}$  can be employed as a constraints for closures.

Although shearing box simulations must be considered with caution in the context of disc modeling for observations, modelers appealing to the MRI and extracting guidance from simulations should treat  $\alpha_{tot}$  and  $\beta$  as dependent parameters. The value of  $\alpha_{tot}\beta \sim 0.4 - 0.5$  which is extracted from Figs. 1 and 2 emerges as a more robust constraint than any specific value of  $\alpha_{tot}$ . A relation between  $\alpha_{tot}$  and  $\beta$  has been incorporated into some disk models (e.g. Narayan et al. 1998) but not others (e.g. Yuan et al. 2005). Note also that the data herein are primarily for thin disks. While similar principles would apply for thick disks, the numerical constant could be different.

**Acknowledgments:** EB thanks V. Pariev and D. Uzdensky for discussions. We acknowledge support from NSF grants AST-0406799, AST 00-98442, AST-0406823, NASA grant ATP04-0000-0016, and the KITP of UCSB, with support from NSF Grant PHY-9907949. We acknowledge support from the Laboratory for Laser Energetics.

## REFERENCES

Blackman, E. G. 1998, MNRAS, 299, L48

Balbus S.A. & Hawley J.F., 1991, ApJ , 376 214.

Balbus, S. A., & Hawley, J. F. 1998, Rev. Mod. Phys., 70, 1

Brandenburg, A., Nordlund, A., Stein, R. F., & Torkelsson, U. 1995, ApJ, 446, 741

Hawley, J.F., Gammie C.F. & Balbus, S.A., 1995, ApJ 440, 742

Hawley, J. F., Gammie, C. F., & Balbus, S. A. 1996, ApJ, 464, 690

Frank J., King A., Raine D., 1992, “Accretion Power in Astrophysics,” (Cambridge: Cambridge Univ. Press).

Narayan, R., Mahadevan, R., & Quataert, E. 1998, in Theory of Black Hole Accretion Disks, edited by Marek A. Abramowicz, Gunnlaugur Bjornsson, and James E. Pringle. Cambridge University Press, 1998., p.148

Ogilvie, G. I. 2003, MNRAS, 340, 969

Pessah, M. E., Chan, C.-k., & Psaltis, D. 2006, submitted to MNRAS, astro-ph/0603178

Pessah, M. E., Chan, C.-k., & Psaltis, D. 2006, submitted to Phys. Rev. Lett.

Schekochihin, A.A., Cowley, S.C., Hammett, G.W., Maron, J.L., & McWilliams, J.C. 2002, New Journal of Physics, 4, 84

Shakura N.I. & Sunyaev R.A., 1973, A& A., 24, 337

Stone, J. M., Hawley, J. F., Gammie, C. F., & Balbus, S. A. 1996, ApJ, 463, 656

Yuan, F., Taam, R. E., Xue, Y., & Cui, W. 2005, ApJ in press,

Table 1. Overview of models

Paper	$\beta$ -range	$\langle\langle\alpha_{\text{mag}}\rangle\rangle$ -range	$\langle\langle\alpha_{\text{kin}}\rangle\rangle$ -range	Vertical density
Hawley et al. 1995	0.0294–76.9	0.002–11.6	0.0004–3.22	unstratified
Brandenburg et al. 1995	20–77	0.0007–0.0041	0.0002–0.0010	stratified
Stone et al. 1996	21.8–250	0.00094–0.00991	0.00032–0.00320	stratified
Hawley et al. 1996	16–250	0.0017–0.0268	0.0007–0.0042	unstratified

Table 2. Hawley et al., 1995. Uniform initial  $\overline{B}_z$  simulations.

Model	$\beta_{\text{init}}^{\text{a}}$	Orbits	$\langle\langle\beta\rangle\rangle^{\text{b},\text{c}}$	$\langle\langle\alpha_{\text{mag}}\rangle\rangle^{\text{d}}$	$\langle\langle\alpha_{\text{kin}}\rangle\rangle^{\text{e}}$
Z3.....	100	3.3	0.0294 <sup>f</sup>	11.6 <sup>f</sup>	3.22 <sup>f</sup>
Z4.....	400	10.7	1.96	0.303	0.070
Z5.....	700	14.8	2.64	0.149	0.059
Z7.....	400	11.9	2.57	0.219	0.064
Z9.....	400	16.3	0.935	0.526	0.117
Z12.....	400	7.5-11.7	1.08	0.480	0.130
Z15.....	400	7.5-11.7	0.769	0.667	0.140
Z17.....	1600	11.4	3.94	0.127	0.030
Z18.....	400	9.5	2.40	0.266	0.117
Z19.....	400	8.9	2.15	0.289	0.080
Z20.....	3200	20.0	7.63	0.061	0.017
Z21.....	3200	11.0	6.54	0.074	0.020
Z22.....	400	7.8	2.60	0.213	0.046
Z23.....	12800	10.7	27.0	0.020	0.004
Z24.....	51200	6.7	76.9	0.006	0.001
Z25.....	51200	28.4	30.3	0.014	0.005
YZ1.....	400 (100) <sup>g</sup>	10.6-14.9	2.97	0.086	0.045
YZ2.....	3200 (100) <sup>g</sup>	21.2	3.94	0.116	0.027

<sup>a</sup>Initial  $\beta \equiv P(\text{gas})/P(\text{magnetic})$ .

<sup>b</sup> $\langle\langle\rangle\rangle$  denotes a time and space average.

<sup>c</sup>This is  $\langle\langle 8\pi P_0/B^2 \rangle\rangle$  from Hawley et al., 1995, where  $P_0 = 10^{-6}$  is the initial pressure.

<sup>d</sup>This is  $\langle\langle -B_x B_y / (4\pi P_0) \rangle\rangle$  from Hawley et al., 1995.

<sup>e</sup>This is  $\langle\langle \rho v_x \delta v_y / P_0 \rangle\rangle$  from Hawley et al., 1995.

<sup>f</sup>Value at end of run.

<sup>g</sup>Combined toroidal and vertical field run.  $\beta(B_y)$  in parenthesis.

ses.

Table 3. Hawley et al., 1995. Uniform initial  $\overline{B}_y$  simulations.

Model	$\beta_{\text{init}}^{\text{a}}$	Orbits	$\langle\langle\beta\rangle\rangle^{\text{b},\text{c}}$	$\langle\langle\alpha_{\text{mag}}\rangle\rangle^{\text{d}}$	$\langle\langle\alpha_{\text{kin}}\rangle\rangle^{\text{e}}$
Y1.....	100	21.2	13.9	0.031	0.010
Y2.....	400	21.7	30.3	0.013	0.004
Y3.....	30	17.0	8.62	0.049	0.016
Y6.....	100	23.7	23.8	0.013	0.005
Y7.....	25	13.3	9.26	0.037	0.010
Y8.....	2	12.6	1.63	0.084	0.022
Y9.....	30	15.9	8.62	0.041	0.010
Y10.....	100	13.9	62.5	0.003	0.001
Y11.....	100	12.0	16.9	0.024	0.008
Y12.....	400	10.0	50.0	0.008	0.003
Y13.....	100	15.8-20.0	14.1	0.030	0.009
Y15.....	100	28.8	8.55	0.047	0.014
Y17.....	1200	13.2	185	0.002	0.0004
Y18.....	10	10.8	3.86	0.098	0.027
YZ1.....	100 (400) <sup>f</sup>	10.6-14.9	2.97	0.086	0.045
YZ2.....	100 (3200) <sup>f</sup>	21.2	3.94	0.116	0.027

<sup>a</sup>Initial  $\beta \equiv P(\text{gas})/P(\text{magnetic})$ .

<sup>b</sup> $\langle\langle \rangle\rangle$  denotes a time and space average.

<sup>c</sup>This is  $\langle\langle 8\pi P_0/B^2 \rangle\rangle$  from Hawley et al., 1995, where  $P_0 = 10^{-6}$  is the initial pressure.

<sup>d</sup>This is  $\langle\langle -B_x B_y / (4\pi P_0) \rangle\rangle$  from Hawley et al., 1995.

<sup>e</sup>This is  $\langle\langle \rho v_x \delta v_y / P_0 \rangle\rangle$  from Hawley et al., 1995.

<sup>f</sup>Combined toroidal and vertical field run.  $\beta(B_y)$  in parentheses.

Table 4. Brandenburg et al., 1995. Initial  $\overline{B}_z$  simulations.

Model	$\beta_{\text{init}}$	$\langle\langle\beta\rangle\rangle^a$	$\langle\langle\alpha_{\text{mag}}\rangle\rangle^a$	$\langle\langle\alpha_{\text{kin}}\rangle\rangle^a$	Cooling	Parity
A	100	77	0.0015	0.0005	Yes	Odd
B	100	71	0.0007	0.0002	Yes	Odd
C	100	20	0.0041	0.0010	Yes	Even
D	100	71	0.0014	0.0003	No	Odd
E1 <sup>b</sup>	100	43	0.0035	0.0005	No	Free
E2 <sup>b</sup>	100	59	0.0023	0.0003	No	Free
AD <sup>c</sup>	100	20	0.0031	0.0007	Yes	Even

<sup>a</sup> $\langle\langle\rangle\rangle$  denotes a time and space average.

<sup>b</sup>Averages are given over the last 3/4 of the run (E1) and over the full run (E2).

<sup>c</sup>Ambipolar diffusion.

Table 5. Stone et al., 1996

Model <sup>a</sup>	$\beta_{\text{init}}$	Orbits	$\langle\langle\beta\rangle\rangle^{\text{bcd}}\langle\langle\alpha_{\text{mag}}\rangle\rangle^{\text{bce}}\langle\langle\alpha_{\text{kin}}\rangle\rangle^{\text{bcf}}$		
IZ1	100	54	65.4	0.00444	0.00125
IZ2	400	54	250.0	0.00097	0.00045
IZ3	25	54	62.9	0.00442	0.00126
IZ6	100	40	49.8	0.00682	0.00190
IY1	100	30	27.9	0.00991	0.00240
IY2	400	30	163.4	0.00094	0.00032
IY3	25	28	25.8	0.00798	0.00206
AZ1	100	50	42.2	0.00766	0.00172
AZ6	100	10	27.2 <sup>g</sup>	0.01420 <sup>g</sup>	0.00320 <sup>g</sup>
AY1	100	40	21.8	0.01220	0.00291
AL6	100	40	58.5	0.00489	0.00119

<sup>a</sup>Runs are labeled with the letter I for isothermal A for adiabatic. Second letter denotes initial configuration of magnetic field: Z = zero-net-Z, Y = pure-Y, L = flux loops.

<sup>b</sup> $\langle\langle\rangle\rangle$  denotes a time and space average.

<sup>c</sup>Time averages begun at orbit 10 for zero-net-Z fields, orbit 15 for pure-Y fields, and orbit 20 for flux loops.

<sup>d</sup>This is  $\langle\langle8\pi P(0)/B^2\rangle\rangle$  from Stone et al., 1996, where  $P(0) = 5 \times 10^{-7}$  is the pressure at the mid-plane.

<sup>e</sup>This is  $\langle\langle-B_x B_y/(8\pi P(0))\rangle\rangle$  from Stone et al., 1996.

<sup>f</sup>This is  $\langle\langle\rho v_x \delta v_y/P(0)\rangle\rangle$  from Stone et al., 1996.

<sup>g</sup>Time average from orbits 5 through 10.

Table 6. Hawley et al., 1996. Random initial  $B$  simulations.

Model	$\beta_{\text{init}}^{\text{a}}$	Orbits	$\langle\langle\beta\rangle\rangle^{\text{bc}}$	$\langle\langle\alpha_{\text{mag}}\rangle\rangle^{\text{bd}}$	$\langle\langle\alpha_{\text{kin}}\rangle\rangle^{\text{bf}}$
R1	800	200	34	0.0122	0.0042
R2	50	50.8	63	0.0066	0.0027
R3	200	50.8	32	0.0136	0.0042
R4	1600	74.9	67	0.0061	0.0025
R6	800	40-74.8	16	0.0268	0.0101
R7	200	52.0	250	0.0017	0.0007

<sup>a</sup>Initial  $\beta \equiv P(\text{gas})/P(\text{magnetic})$ .

<sup>b</sup> $\langle\langle\rangle\rangle$  denotes a time and space average.

<sup>c</sup>This is  $\langle\langle 8\pi P_0/B^2 \rangle\rangle$  from Hawley et al., 1996, where  $P_0$  is the initial (and final) thermal pressure.

<sup>d</sup>This is  $\langle\langle -B_x B_y/(4\pi P_0) \rangle\rangle$  from Hawley et al., 1996.

<sup>e</sup>This is  $\langle\langle \rho v_x \delta v_y / P_0 \rangle\rangle$  from Hawley et al., 1996.

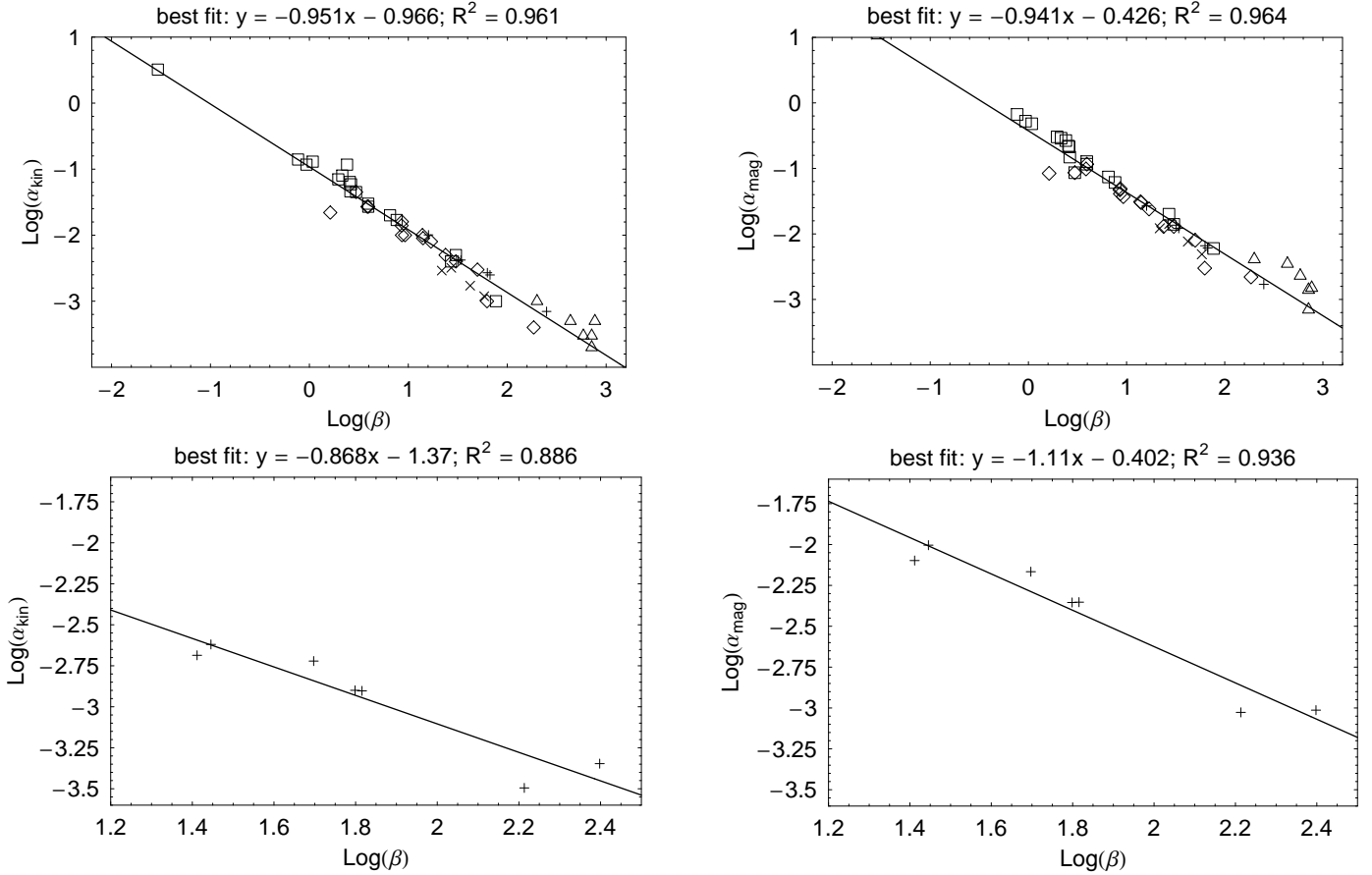


Fig. 1.— Plots of  $\text{Log } \alpha_{\text{kin}}$  and  $\text{Log } \alpha_{\text{mag}}$  vs  $\text{Log}(\beta)$  using the data of Tables 2-5, extracted from published simulations. In all panels, triangles are Brandenburg et al. 1995 (Table 4); Diamonds are Hawley et al. 1995 with initial  $\bar{B}_y$  (Table 3) squares are Hawley et al. 1995, with initial  $\bar{B}_z$  (Table 2); Crosses are Stone et al. 1996 (Table 5); Plusses are Hawley, Gammie, and Balbus 1996 (Table 6). The top rows show simulations with  $\Gamma = 5/3$  (adiabatic) and the bottom row shows simulations with  $\Gamma = 1$  (isothermal). Despite the different initial conditions and boundary conditions and widely ranges of  $\alpha_{\text{mag}}$ ,  $\alpha_{\text{kin}}$ , and  $\alpha_{\text{tot}}$ , the products  $\alpha\beta$  are largely conserved. The best fits to the data are the solid lines shown, with the equations of those lines at the top of each panel with the square of correlation coefficient  $R^2$  shown

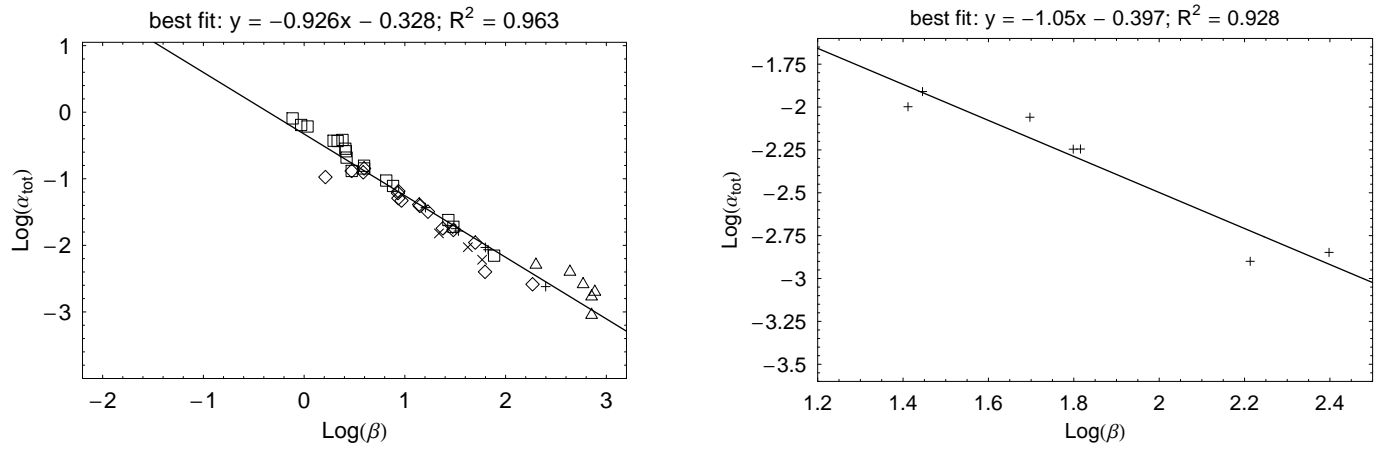


Fig. 2.— Same as Fig. 1 but for plots of  $\text{Log} \alpha_{\text{tot}}$  and  $\text{Log} \alpha_{\text{tot}}$  vs  $\text{Log}(\beta)$ . Left:  $\Gamma = 5/3$  (adiabatic), Right:  $\Gamma = 1$  (isothermal)